

# Investigation and prediction of springback in rotary-draw tube bending process using finite element method

Proc IMechE Part C:  
*J Mechanical Engineering Science*  
226(12) 2967–2981  
© IMechE 2012  
Reprints and permissions:  
sagepub.co.uk/journalsPermissions.nav  
DOI: 10.1177/0954406212440672  
pic.sagepub.com



Levent Sözen, Mehmet A Guler, Deniz Bekar and Erdem Acar

## Abstract

Rotary-draw tube bending operation is one of the most universal methods used for the tube forming processes. Similar to the other forming methods, some problems such as wall thinning, cross-section distortion, wrinkling, and springback can also be seen on the tubes formed by rotary-draw bending operations. Springback is a very common problem and its prediction plays a crucial role in increasing the efficiency of the tube bending operations and also to overcome the difficulties in the assembly processes. Tube diameter, wall thickness, bend radius, bend angle, and coefficient of friction can be considered as the most effective parameters that cause the variation of springback magnitude. In this study, not a simple one-at-a-time sensitivity analysis, but a thorough investigation of the springback phenomena involving interactions between the geometrical and mechanical parameters is done and surrogate models are developed via the data obtained from finite element analysis using a multi-purpose explicit and implicit finite element software LS-DYNA to analyze the non-linear response of structures. The constructed surrogate models can be utilized to perform fast prediction of springback for a given combination of parameters. Three different surrogate modeling techniques are exploited and it is found that the linear polynomial response surface approximations can provide acceptable accuracy. Finally, experiments are conducted to validate the accuracy of surrogate models. It is observed that the cross-validation error predictions are close to the errors observed in the experiments.

## Keywords

Rotary-draw tube bending, springback, thin-walled tube, surrogate models, analysis of variance, Taguchi orthogonal arrays, finite element analysis

Date received: 9 December 2011; accepted: 8 February 2012

## Introduction

Tube bending operation is a manufacturing process, which has a wide range of applications in many industries including automotive, aerospace, shipping, construction, furniture, etc. The tube bending operations are performed using tube bending machines, which have become widespread as the computer numerical control (CNC) technology is integrated with them. Although there are various types of tube bending processes, such as rotary-draw, compression, ram, press, and roll bending, the rotary-draw tube bending operation is the most common method and can handle about 95% of tube bending operations.<sup>1</sup> Thin-walled tubes can be easily bent in desired small radii using a rotary-draw tube bending machine; moreover, low operating costs and high tooling variety are the most obvious advantages of this bending method.<sup>2</sup> A typical

CNC rotary-draw tube bending machine includes five main bending components, as shown in Figure 1. These are: (i) the bend die, (ii) the bend die assistant, (iii) the clamp die, (iv) the wiper die, and (v) the pressure die.

The rotary-draw tube bending operation has been investigated using analytical, numerical as well as the experimental methods in various studies. Pan and Stelson<sup>3</sup> explored the relation between bend radius and cross-section deformation for tube bending operations using analytical methods. A comprehensive

---

Department of Mechanical Engineering, TOBB University of Economics and Technology, Turkey

### Corresponding author:

Mehmet A Guler, Department of Mechanical Engineering, TOBB University of Economics and Technology, Ankara 06560, Turkey.  
Email: mguler@etu.edu.tr

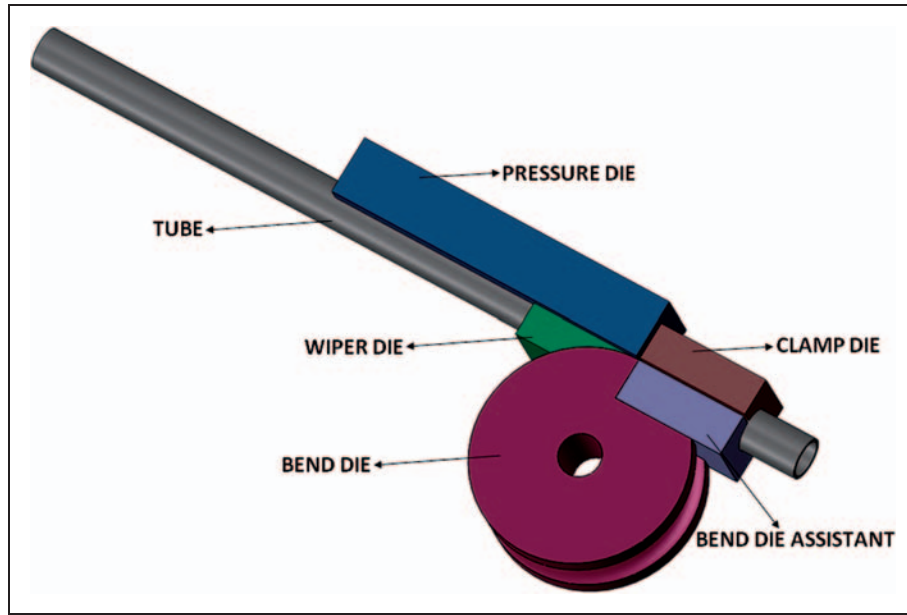


Figure 1. Components of rotary-draw tube bender.

Table 1. Geometrical properties for validation model.

|                                   |     |
|-----------------------------------|-----|
| Outside diameter of the tube (mm) | 20  |
| Thickness of the tube (mm)        | 1.5 |
| Bend radius (mm)                  | 50  |
| Clamp die length (mm)             | 55  |
| Pressure die length (mm)          | 160 |
| Wiper die length (mm)             | 55  |

Table 2. Mechanical properties. Data from<sup>6</sup>

| Material                | Steel A573-81 65 |
|-------------------------|------------------|
| Yield strength (MPa)    | 270              |
| Tangent modulus (MPa)   | 900              |
| Young's modulus (MPa)   | 219,400          |
| Poisson's ratio         | 0.3              |
| Coefficient of friction | 0.3              |

study was performed by Shr<sup>4</sup> that included experimental, analytical, and numerical studies about thickness reduction, surface strain distribution, and springback occurrence for rotary-draw tube bending operations. Khodayari<sup>5</sup> experimentally examined thickness distribution, amount of ovality, and springback for two different types of materials using rotary-draw tube bending machine. Wang and Agarwal<sup>6</sup> modified the

rotary-draw tube bending operations by applying axial pull and internal pressure in order to reduce cross-section distortion and wrinkling.

Rotary-draw tube bending process is also used as a pre-form operation before hydroforming, which is generally used in order to obtain complex tube geometries. The success of the hydroforming operations widely depends on the quality of pre-bent operations often applied prior to hydroforming.<sup>7</sup> Grantab<sup>8</sup> studied crashworthiness of hydroformed tube geometries and also performed the rotary-draw tube bending experiments and simulations. Sorine<sup>9</sup> also analyzed pre-forming and hydroforming operations performed on advanced high strength steel tubes using experimental and numerical methods. Li et al.<sup>10</sup> performed a numerical study on the effect of mandrel on stress distribution to reveal wrinkling using both stainless steel and aluminum rotary-draw bend tubes. The deformation behavior of the tubes which have large diameter, and a small bending radius is also investigated by the help of an analytical model and series of finite element (FE) models in order to observe the bending capacity of the tubes with respect to wrinkling, wall thinning, and cross-section deformation.<sup>11</sup> Another study, which focuses on wrinkling problem occurring in rotary-draw bending operation, is performed by Yang et al.<sup>12</sup> They studied on prediction of wrinkling for the large diameter aluminum alloy thin-walled tubes depending on diameter, clearances and coefficient of friction. For the rotary-draw bending operations, not only circular formed geometries, but also rectangular formed ones are also investigated by the help of finite

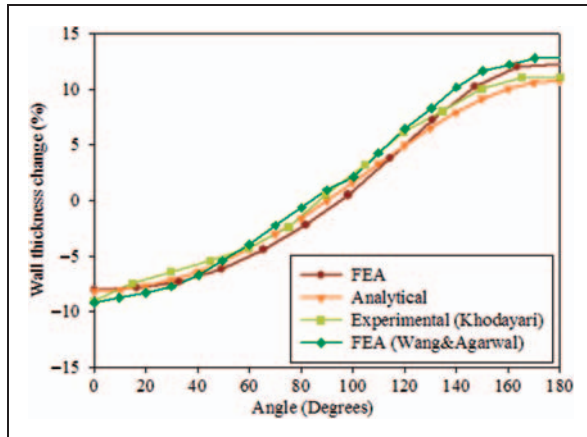


Figure 2. Wall thickness change.

element analysis (FEA). In this field, Zhao et al.<sup>13</sup> performed three-dimensional FE simulations for rectangular shaped aluminum tubes in order to obtain the tangential stress distribution.<sup>13</sup> It should be noted that instead of using the FE method, meshfree methods can also be used to perform springback prediction in tube bending and forming process. There exist several studies including Song et al.<sup>14</sup> and Liu et al.<sup>15</sup> that showed that the meshfree methods can provide more accurate results for springback analysis in sheet metal forming.

There are some fundamental studies about springback problem in tube forming operations that are worth mentioning. The most comprehensive study was performed by Gu et al., where the effects of parameters are investigated using a one-at-a-time (OAT) sensitivity analysis.<sup>16</sup> The effect of mandrel on the occurrence of springback is also investigated and the whole process is analyzed in three steps: (1) bending the tube, (2) retracting the mandrel, and (3) springback.<sup>17</sup> The parameters that affect the amount of springback angle are also investigated by Da-xin et al.<sup>18</sup> The results show that mechanical properties of the materials, the bend radius, and the wall thickness should be considered while determining the springback angle. The studies also revealed that springback occurrence can be compensated online by the help of the adaptive bend correction algorithm. This algorithm stores online measurements in each step and modifies the updated bends in order to reduce springback occurrence according to the previous bend values.<sup>19,20</sup>

The aforementioned studies generally focused on forming processes and investigated geometrical problems such as cross-section deformation, surface thinning, and wrinkling occurrence. On the other hand, the studies related to the springback occurrence generally focused on the fundamental forming parameters such as the material properties, the tube thickness, the

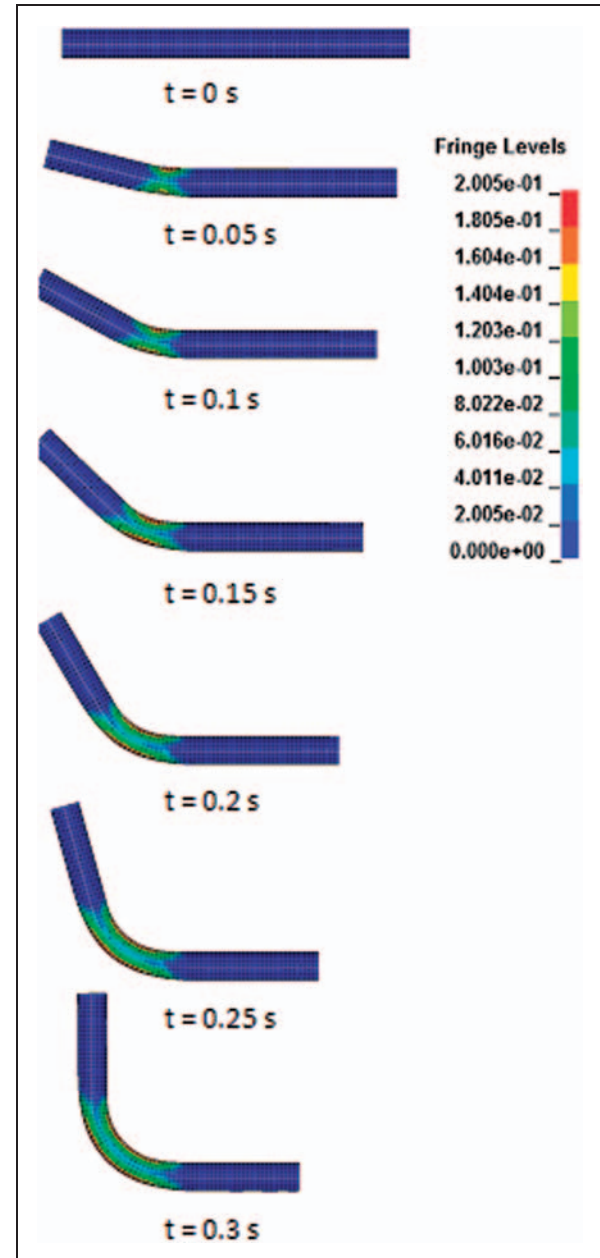


Figure 3. Effective plastic strain contours at different stages of rotary-draw tube bending. Bend radius ( $R$ ): 50 mm, tube diameter ( $D$ ): 20 mm, and tube thickness ( $t$ ): 1.5 mm.

bend angle, and the bend radius. The prediction of springback before the beginning of the bending operation stands out as a topic which has not been adequately studied. Although there are some parametrical studies about occurrence of springback,<sup>16,17</sup> they are generally performed using a OAT sensitivity analysis. In OAT analysis, each variable is changed between its corresponding limits while the other parameters are kept constant at their nominal values. There are two major drawbacks of this approach: (1) the computed sensitivities are local and

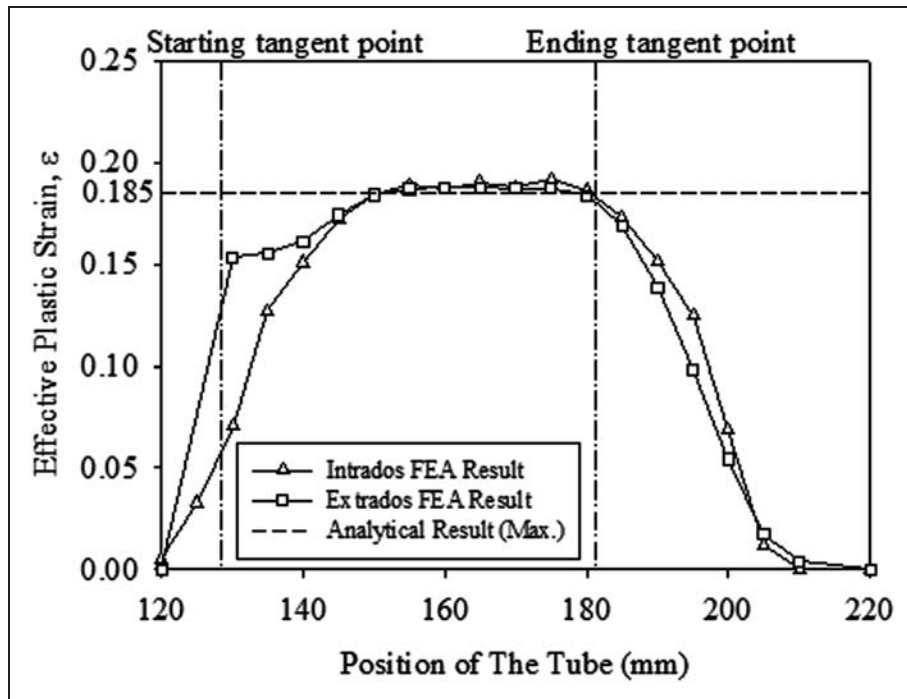


Figure 4. Effective plastic strain distribution at the extrados and intrados segments.

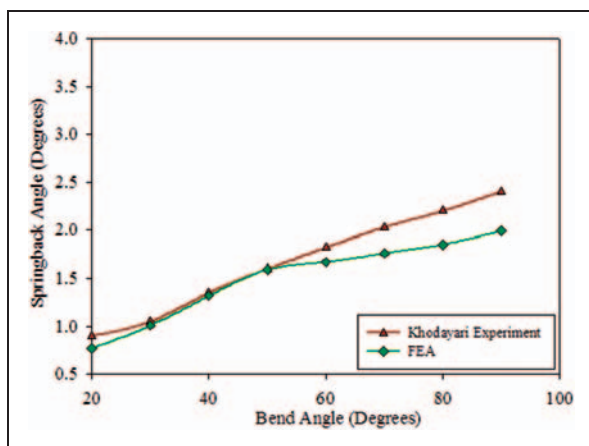
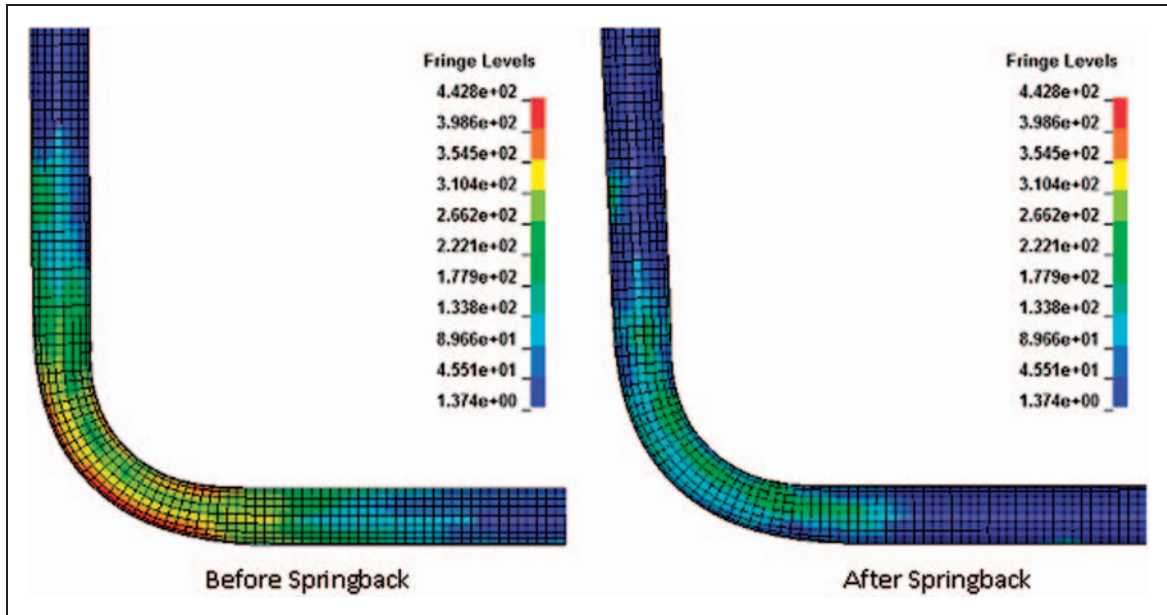


Figure 5. Simulation and experimental results for springback angles.

(2) the interactions between the variables are ignored. To overcome these drawbacks, we perform the sensitivity analysis using analysis of variance (ANOVA) techniques that can provide global sensitivities and can handle variable interactions. In addition, surrogate modeling techniques are utilized to generate approximate models that can mimic the behavior of FEA models and can provide fast prediction of springback for a given combination of process variables. In this study, the diameter of the tube ( $D$ ), the tube thickness ( $t$ ), the ratio of bend radius to the tube diameter ( $R/D$ ),

the bend angle ( $\theta$ ), and the coefficient of friction between the dies and the tube ( $f_s$ ) are considered as fundamental process variables affecting the occurrence of springback.

The study of the springback prediction includes two main steps in our methodology. First, springback values are obtained using FEA for various combinations of forming and geometrical parameters, which are considered as effective on formation of the springback. These combinations of parameters are determined using Taguchi techniques to keep the computational cost at a minimum. Note that prediction of springback by experimental methods is considered as a time-consuming and costly procedure, and FEA provides us the achievement of different bending simulations for various parameters in a cost-effective manner. In the second step, approximate models are generated using the results obtained from the FEA using three well-known surrogate modeling techniques—polynomial response surface (PRS), radial basis functions (RBF), and Kriging (KR). While constructing the surrogate models, the following procedure is pursued. First, ANOVA techniques are utilized to perform a main effects analysis to determine the most influential parameters of the rotary-draw tube bending process. Then, the training point data and the springback values, calculated at the training points, are used to construct surrogate models to build a functional relationship between the springback and the



**Figure 6.** Effective stress contours before and after springback. Material: A573-81 65, bend angle ( $\theta$ ):  $90^\circ$ , bend radius ( $R$ ): 50 mm, tube diameter ( $D$ ): 20 mm, and tube thickness ( $t$ ): 1.5 mm.

problem parameters. Once constructed, these surrogate models provide a very quick springback prediction for any combination of problem parameters.

### Finite element analysis

The rotary-draw tube bending simulations are performed on the basis of real bending operations. The functions of the main components of a rotary-draw tube bending machine should be well understood before exploring the FEA. Therefore, in this section, a brief description of the rotary-draw tube bending process is given before describing the details of the FEA of the forming and springback simulations. A typical rotary-draw bending operation can be described as follows: prior to the bending process, the bend die assistant, the clamp die, and the tube are aligned with the feeding axes, and then the clamp die is engaged with the bend die assistant in order to prevent sliding of the tube during the bending operation. The operation starts with the rotation of the bend die. In this way, the bend die assistant and clamp die draw the tube with the bend die and against the pressure die. This movement provides plastic deformation both at intrados and extrados segments of the tube. The pressure die provides an additional moment in order to help completing the bending operation and it also reduces the section thinning.<sup>4</sup> The main purpose of using the wiper die is to provide additional support to the tube behind the tangent point of the bend and it helps to prevent wrinkling at the intrados of the tube.<sup>2</sup> The wiper die also minimizes frictional drag during the bending operation.<sup>8</sup> An internal

mandrel should be used for the operations, which include larger diameter and thin-walled tubes to substantially prevent cross-section deformation and to reduce ovality. Based on the values of the thickness and the diameter of the tube, bend tooling can be equipped with a plug or 1–3 balls of mandrel.<sup>8</sup>

### Forming simulation

FE model of the rotary-draw tube bending operation is prepared in ANSA<sup>21</sup> and validated with the analytical and experimental studies cited in the literature.<sup>4,5</sup> Solid model of the tube and bend tools are prepared according to the geometrical properties of Khodayari's<sup>5</sup> experimental study, the parameters of which are given in Table 1. In the FEA model, 3 mm element mesh size is considered to be reasonable after the mesh convergence studies. Belytschko-Tsay shell element with 10 integration points along the thickness is used in the FEA.

The accuracy of the springback simulations are highly dependent on forming simulations, which are performed explicitly using the non-linear explicit FE code LS-DYNA.<sup>22</sup> In the explicit forming simulations, determining the most appropriate tooling velocity is essential in order to reduce the simulation time and the artificial dynamic effects.<sup>23</sup> The tube material is modeled as 'Piecewise Linear Plastic' using MAT-024 model from the LS-DYNA material library. Table 2 lists the material model parameters, which include the Young's modulus, the tangent modulus, the yield strength, and the Poisson's ratio. Bend tools are

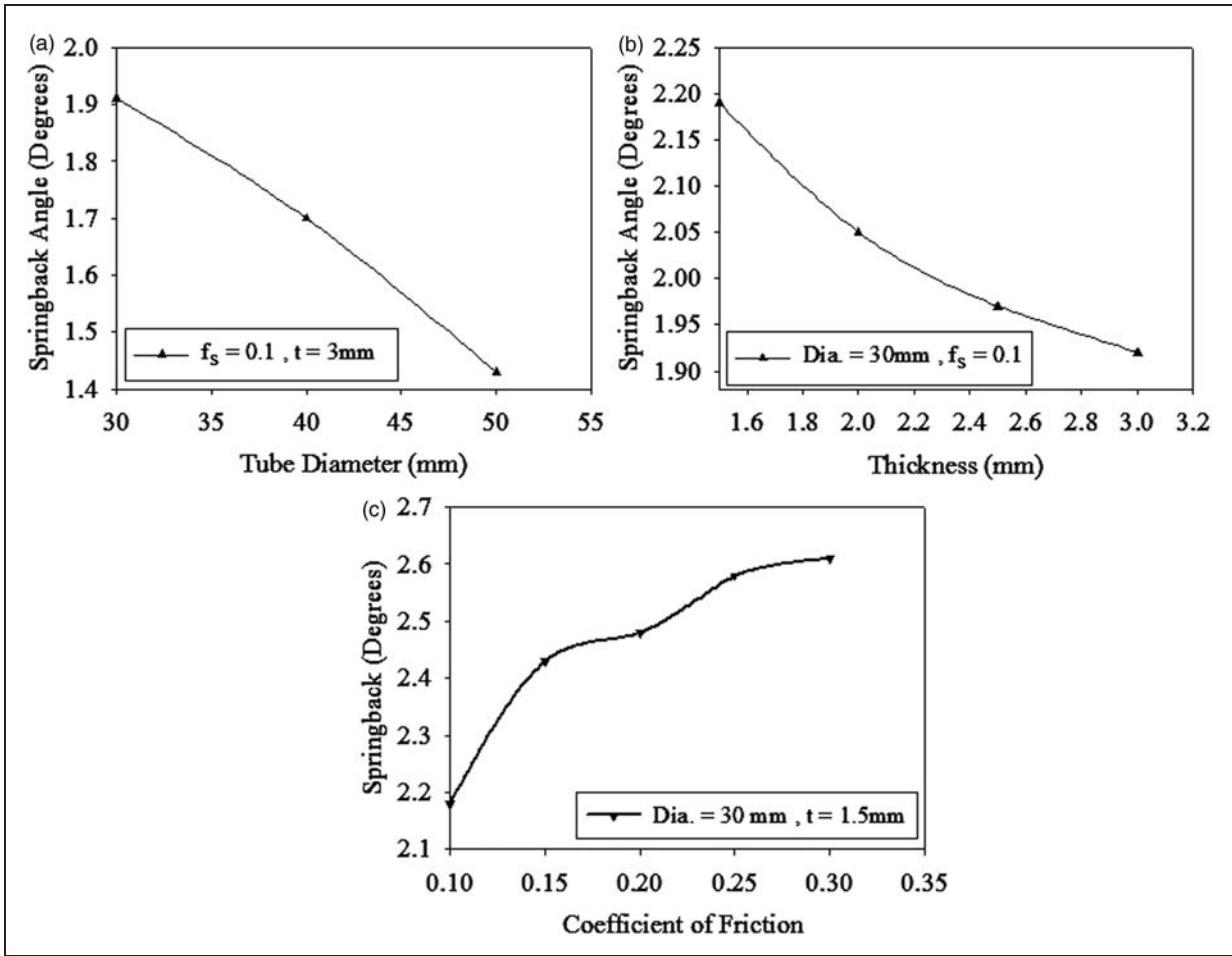


**Figure 7.** Springback angle depending on: (a) the diameter of the tube ( $D$ ), (b) the thickness of the tube ( $t$ ), and (c) the coefficient of friction ( $f_s$ ).

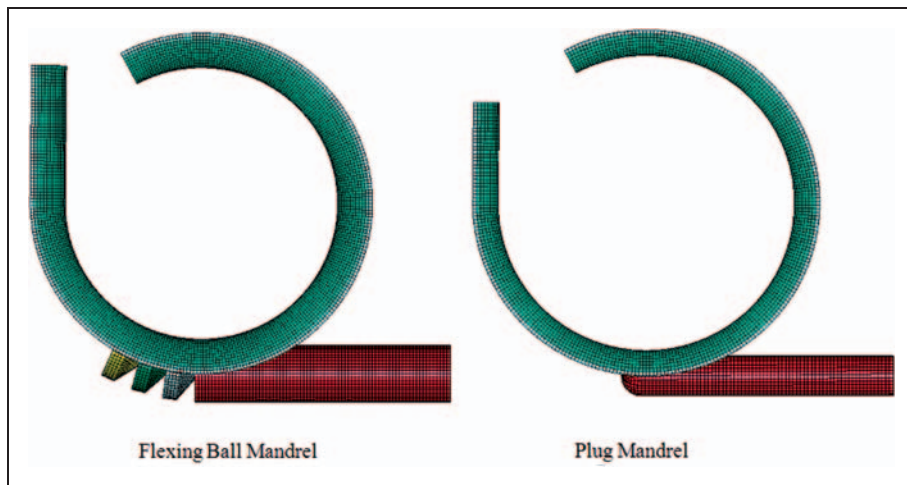


**Figure 8.** Types of mandrels used.

**Table 3.** Geometrical properties of the training models (L25-Taguchi array).

| Model | D (mm) | R (mm) | Clamp die (mm) | Pressure die (mm) | Wiper die (mm) | Mandrel | Tangent length (mm) |
|-------|--------|--------|----------------|-------------------|----------------|---------|---------------------|
| 1     | 30     | 60.0   | 60             | 100               | 51             | RP-2    | 4.8                 |
| 2     | 30     | 75.0   | 60             | 150               | 51             | RP-1    | 4.8                 |
| 3     | 30     | 90.0   | 60             | 200               | 51             | P       | 4.8                 |
| 4     | 30     | 105.0  | 60             | 250               | 51             | –       | 4.8                 |
| 5     | 30     | 120.0  | 60             | 300               | 51             | –       | 4.8                 |
| 6     | 40     | 100.0  | 80             | 200               | 64             | RP-2    | 3.9                 |
| 7     | 40     | 120.0  | 80             | 300               | 64             | RP-1    | 3.9                 |
| 8     | 40     | 140.0  | 80             | 350               | 64             | P       | 3.9                 |
| 9     | 40     | 160.0  | 80             | 200               | 64             | –       | 3.9                 |
| 10    | 40     | 80.0   | 80             | 200               | 64             | RP-2    | 3.9                 |
| 11    | 50     | 150.0  | 100            | 400               | 76             | RP-2    | 4.8                 |
| 12    | 50     | 175.0  | 100            | 200               | 76             | P       | 4.8                 |
| 13    | 50     | 200.0  | 100            | 300               | 76             | –       | 4.8                 |
| 14    | 50     | 100.0  | 100            | 250               | 76             | RP-3    | 4.8                 |
| 15    | 50     | 125.0  | 100            | 300               | 76             | RP-2    | 4.8                 |
| 16    | 60     | 210.0  | 120            | 350               | 76             | RP-1    | 5.8                 |
| 17    | 60     | 240.0  | 120            | 400               | 76             | RP-1    | 5.8                 |
| 18    | 60     | 120.0  | 120            | 350               | 76             | CP-4    | 4.8                 |
| 19    | 60     | 150.0  | 120            | 400               | 76             | RP-3    | 5.8                 |
| 20    | 60     | 180.0  | 120            | 250               | 76             | RP-3    | 5.8                 |
| 21    | 70     | 280.0  | 140            | 550               | 102            | RP-1    | 6.4                 |
| 22    | 70     | 140.0  | 140            | 450               | 102            | CP-4    | 5.8                 |
| 23    | 70     | 175.0  | 140            | 250               | 102            | CP-4    | 5.8                 |
| 24    | 70     | 210.0  | 140            | 350               | 102            | RP-3    | 6.4                 |
| 25    | 70     | 245.0  | 140            | 450               | 102            | RP-1    | 6.4                 |

P: Plug mandrel; RP-N: Regular pitch 'N' numbered ball mandrel; CP-N: Close pitch 'N' numbered ball mandrel.

modeled as rigid materials using the material model MAT-20 from the LS-DYNA material library. The contact between the tube and the bend dies are modeled using the surface-to-surface contact algorithm using the 'CONTACT\_ONE\_WAY\_SURFACE\_TO\_SURFACE' keyword and the frictional effects are included by selecting the friction coefficient as 0.3, which is consistent with the validation case study. The validation run is performed for a 90° of bend angle.

In Figure 2, the change in the wall thickness is plotted using the data obtained from the segment of the tube having 45° of angle with respect to the feeding axes. The outcomes are compared with the analytical results obtained the expression given by Shr,<sup>4</sup> the experimental data of Khodayari<sup>5</sup> and the FEA results of Wang.<sup>6</sup> When the change in the wall thickness graph is examined, a sufficient agreement was observed between the experimental and simulation results and thus, we concluded that the

FE model used in this study is reliable and sufficiently accurate.

Another decisive parameter for the determination of the accuracy of the FEA model is to compare the effective plastic strain distribution of the FE model with the corresponding analytical calculations. The plastic strain, which causes permanent deformation of the tube, can be obtained both analytically and numerically. Effective plastic strain contour plot obtained from FEA is given in Figure 3 for seven different time steps in series and the analytical data of the effective plastic strain are obtained from the expression given by Shr.<sup>4</sup> The simulation results are given for both extrados and intrados segments. In Figure 4, the comparison results for the effective plastic strain distribution at the extrados and intrados segments of the tube, which is measured at the end of the 90° of angle bending simulation, is given. It should be noted in this comparison that an

**Table 4.** Springback results corresponding to the training points.

| Number | Diameter, D (mm) | Thickness, t (mm) | R/D | Bend angle (°) | Friction | Springback (°) |
|--------|------------------|-------------------|-----|----------------|----------|----------------|
| 1      | 30               | 1.5               | 2   | 30             | 0.05     | 1.09           |
| 2      | 30               | 2                 | 2.5 | 45             | 0.1      | 1.05           |
| 3      | 30               | 3                 | 3   | 60             | 0.15     | 1.38           |
| 4      | 30               | 4                 | 3.5 | 75             | 0.2      | 1.65           |
| 5      | 30               | 6                 | 4   | 90             | 0.25     | 1.41           |
| 6      | 40               | 1.5               | 2.5 | 60             | 0.2      | 1.01           |
| 7      | 40               | 2                 | 3   | 75             | 0.25     | 1.43           |
| 8      | 40               | 3                 | 3.5 | 90             | 0.05     | 1.68           |
| 9      | 40               | 4                 | 4   | 30             | 0.1      | 1.01           |
| 10     | 40               | 6                 | 2   | 45             | 0.15     | 1.04           |
| 11     | 50               | 1.5               | 3   | 90             | 0.1      | 0.94           |
| 12     | 50               | 2                 | 3.5 | 30             | 0.15     | 0.96           |
| 13     | 50               | 3                 | 4   | 45             | 0.2      | 1.28           |
| 14     | 50               | 4                 | 2   | 60             | 0.25     | 0.89           |
| 15     | 50               | 6                 | 2.5 | 75             | 0.05     | 1.06           |
| 16     | 60               | 1.5               | 3.5 | 45             | 0.25     | 1.05           |
| 17     | 60               | 2                 | 4   | 60             | 0.05     | 1.17           |
| 18     | 60               | 3                 | 2   | 75             | 0.1      | 0.87           |
| 19     | 60               | 4                 | 2.5 | 90             | 0.15     | 1.15           |
| 20     | 60               | 6                 | 3   | 30             | 0.2      | 0.68           |
| 21     | 70               | 1.5               | 4   | 75             | 0.15     | 0.63           |
| 22     | 70               | 2                 | 2   | 90             | 0.2      | 0.93           |
| 23     | 70               | 3                 | 2.5 | 30             | 0.25     | 0.77           |
| 24     | 70               | 4                 | 3   | 45             | 0.05     | 1.04           |
| 25     | 70               | 6                 | 3.5 | 60             | 0.1      | 0.78           |

**Table 5.** ANOVA table.

| Source     | Sum of squares | d.f. | Mean squares | F    | p > F  | Effect (%) |
|------------|----------------|------|--------------|------|--------|------------|
| D          | 0.77012        | 4    | 0.19253      | 10.4 | 0.0218 | 43.76      |
| t          | 0.22368        | 4    | 0.05592      | 3.01 | 0.1553 | 12.71      |
| R/D        | 0.19976        | 4    | 0.04994      | 2.69 | 0.1805 | 11.35      |
| Bend angle | 0.27716        | 4    | 0.06929      | 3.73 | 0.1150 | 15.75      |
| Friction   | 0.21484        | 4    | 0.05371      | 2.89 | 0.1640 | 12.21      |
| Error      | 0.07424        | 4    | 0.01856      |      |        |            |
| Total      | 1.75980        | 24   |              |      |        |            |

ANOVA: analysis of variance.

analytical result shows the maximum value of the effective plastic strain at the extrados segment of the tube.

For both the extrados and intrados segments, measurements show good agreement with the analytically calculated maximum plastic strain values.

### Springback simulation

Springback is defined as the deviation from the pre-defined bend angle after the bending operations. The reversion of the elastically deformed part of the tube is considered as the main cause of the springback. In this study, springback simulations are performed implicitly using 'DYNAIN' springback method in LS-DYNA. This method is applied by the help of a file, which includes strain and stress data of the tube's deformed elements. For the implicit springback simulations, double precision version of the LS-DYNA is used in order to obtain a better convergence. Obtaining acceptable springback values depends on the load steps used in the springback simulation. In this study, springback is calculated in every 10 load steps. 'IMPLICIT\_STABILIZATION' keyword is required for the implicit springback simulations in order to extend springback occurrence into several steps and the scale factor is chosen as 0.1 to allow the bent tube springback freely over the first steps. Fully integrated shell element with 10 integration points is used for the springback simulation of the validation model.

Springback simulations were performed for A573-81 65 steel alloy using the geometrical and mechanical properties given in Tables 1 and 2, respectively. Figure 5 shows the comparison between Khodayari's<sup>5</sup> experimental results and our simulation springback results for different bend angles. Springback angles obtained from FEA show reasonable agreement with the experimental results for A573-81 65. Therefore, the springback model can be conveniently applied to the parametric springback study. Effective stress contours are also plotted before and after the implicit springback simulations for the A573-81 65 steel in Figure 6.

### Parametrical study

Since there are various parameters including bend angle, bend radius, tube diameter, thickness, and coefficient of friction, analyzing the effect of combination of these parameters on springback is a cumbersome process. Thus, a preliminary examination is conducted, which included examination of a baseline case and deviation of each individual parameter from the baseline case. Later on, combinations of the parameters are systematically changed and a mathematical expression is developed using the data obtained from the simulations performed in LS-DYNA.

Bend angle is one of the most effective parameters that determine the amount of the elastic strain during the simulation. Figure 5 shows the effect of bend angle on the occurrence of the springback. It is clearly seen

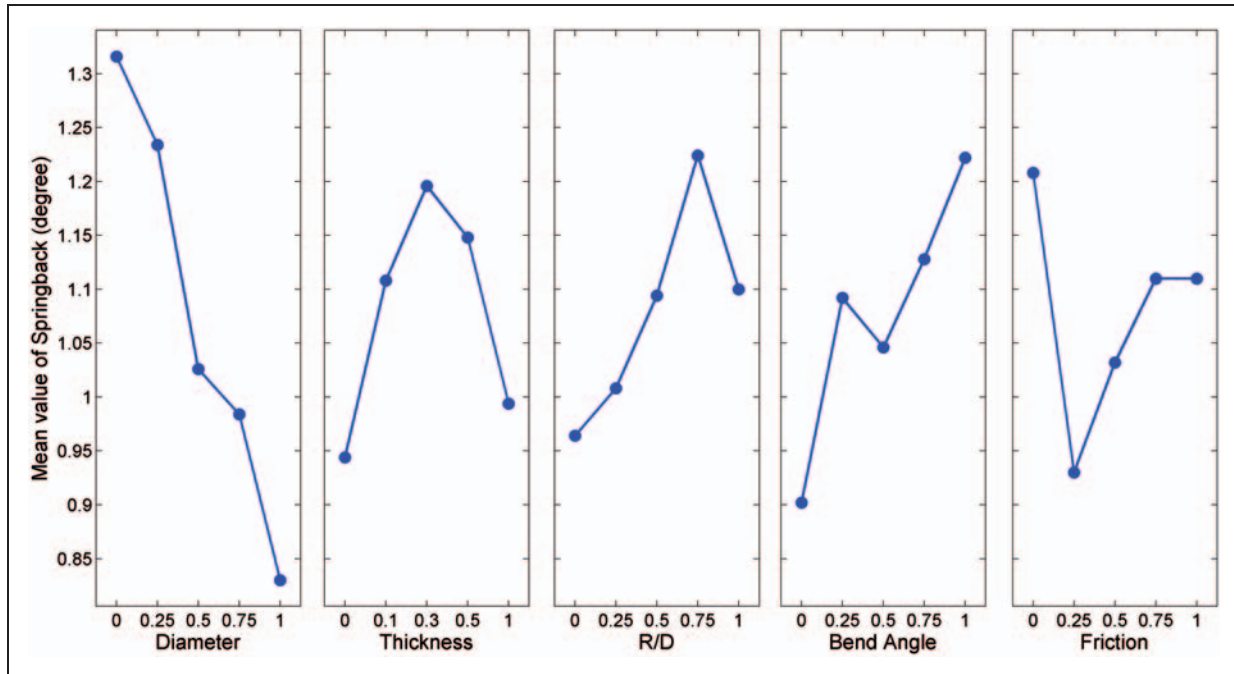


Figure 9. Main effects plot for springback.

Table 6. Geometric properties of the test models.

| Model | D (mm) | R (mm) | Clamp die (mm) | Pressure die (mm) | Wiper die (mm) | Mandrel | Tangent length (mm) |
|-------|--------|--------|----------------|-------------------|----------------|---------|---------------------|
| 26    | 34     | 86.1   | 68             | 200               | 64             | RP-1    | 4.8                 |
| 27    | 44     | 137.4  | 88             | 300               | 76             | RP-1    | 4.8                 |
| 28    | 66     | 234.8  | 132            | 500               | 102            | RP-1    | 6.4                 |
| 29    | 50     | 195.6  | 100            | 250               | 76             | P       | 4.8                 |
| 30    | 60     | 138.9  | 120            | 250               | 76             | RP-3    | 5.8                 |
| 31    | 54     | 216.0  | 108            | 300               | 76             | RP-1    | 5.8                 |
| 32    | 38     | 129.2  | 76             | 150               | 64             | P       | 3.9                 |
| 33    | 32     | 89.6   | 64             | 200               | 51             | P       | 4.8                 |
| 34    | 57     | 165.3  | 114            | 400               | 76             | RP-3    | 5.8                 |
| 35    | 63     | 132.3  | 126            | 400               | 102            | CP-4    | 4.8                 |

P: Plug mandrel; RP-N: Regular pitch 'N' numbered ball mandrel; CP-N: Close pitch 'N' numbered ball mandrel.

that increasing the bend angle causes higher springback angles.

Tube diameter is considered as another very effective parameter linked to the occurrence of the springback. Figure 7(a) shows the change of the springback angle depending on the various bent tube diameter values, while the thickness and friction coefficient are assumed to be constant. Simulations performed for three different diameters (i.e. 30, 40, and 50 mm) show that increasing the diameter of the tube reduces the springback.

Forming and springback simulations are also performed for different thickness values and the results are given in Figure 7(b). Tube diameter and coefficient of friction are considered to be constant and taken as 30 mm and 0.1, respectively. The bending simulations, which have 90° of bend angle, show that increasing the thickness value reduces the springback angle almost linearly.

Springback angle is also affected by changing the coefficient of friction between the dies and the tube. Simulations are performed for 90° of bend angle

while keeping the tube diameter and thickness constant. In Figure 7(c), it is clearly seen that increasing the friction coefficient from the values 0.10 to 0.15 increases the springback angle significantly; however, higher coefficient of friction values leads to smaller amount of increase on springback angle.

To observe the combined effect of the parameters mentioned above, ANOVA techniques are utilized. For that purpose, 25 different FE models having different geometrical and forming properties are prepared. The models, which include large diameter thin-walled tubes, should be equipped with an internal mandrel in order to prevent the wall from collapsing during the bending simulation. Depending on the diameter of the tube, different types of mandrels, which are shown in

Figure 8, are used. For the flexible ball mandrel, 'CONSTRAINED\_JOINT\_SPHERICAL' keyword is used to provide spherical movement ability to the balls. Dimension of the dies and the geometrical properties of the internal mandrels are designed using the data obtained from Miller's<sup>1</sup> guide and they are also given in Table 3 for clarity.

Explicit forming and implicit springback simulations are performed for 25 training points generated using Taguchi orthogonal arrays given in Table 3. A573-81 65 steel, for which the mechanical properties are given in Table 2, is used as a material for the simulations. Springback values for each model are measured and given in Table 4.

### Determination of the most influential parameters

ANOVA is carried out to determine the effects of the input variables on the springback value. Table 5 represents the ANOVA results generated using 'anovan' built-in function of MATLAB<sup>24</sup> that performs multi-way ANOVA for testing the effects of multiple factors on the mean of the springback values. It is found that

**Table 7.** Test points.

| Test points | Diameter, D (mm) | Thickness, t (mm) | Bend R/D | angle (°) | Friction (°) | Springback |
|-------------|------------------|-------------------|----------|-----------|--------------|------------|
| t1          | 32               | 4.2               | 2.8      | 65        | 0.25         | 1.19       |
| t2          | 34               | 4.4               | 2.5      | 59        | 0.21         | 1.40       |
| t3          | 38               | 2.7               | 3.4      | 30        | 0.15         | 0.99       |
| t4          | 44               | 5.4               | 3.1      | 72        | 0.05         | 1.13       |
| t5          | 50               | 3.8               | 3.9      | 31        | 0.13         | 0.91       |
| t6          | 54               | 5.8               | 4        | 43        | 0.07         | 1.06       |
| t7          | 57               | 1.5               | 2.9      | 75        | 0.2          | 0.93       |
| t8          | 60               | 1.9               | 2.3      | 45        | 0.09         | 0.96       |
| t9          | 63               | 4.8               | 2.1      | 90        | 0.12         | 0.93       |
| t10         | 66               | 2.9               | 3.6      | 81        | 0.24         | 1.48       |

**Table 9.** Error metrics for surrogate models.

|      | Linear PRS | Quadratic PRS | RBF  | KR   |
|------|------------|---------------|------|------|
| RMSE | 14.2       | 38.3          | 16.3 | 14.2 |
| MAE  | 12.1       | 31.5          | 14.5 | 12.1 |

PRS: polynomial response surface; RBF: radial basis functions; KR: Kriging; RMSE: root mean square error; MAE: mean absolute error.

**Table 8.** Computed springback values (°) and errors (%) at the test points.

| Test points | Linear PRS              |                         |           | Quadratic PRS           |           | RBF                     |           | KR                      |           |
|-------------|-------------------------|-------------------------|-----------|-------------------------|-----------|-------------------------|-----------|-------------------------|-----------|
|             | Springback <sup>a</sup> | Springback <sup>b</sup> | Error (%) |
| t1          | 1.19                    | 1.30                    | 8.99      | 0.71                    | 40.16     | 1.38                    | 16.14     | 1.30                    | 8.99      |
| t2          | 1.4                     | 1.22                    | 13.43     | 0.58                    | 58.63     | 1.23                    | 13.08     | 1.22                    | 13.43     |
| t3          | 0.99                    | 1.13                    | 14.04     | 0.95                    | 3.98      | 1.05                    | 5.64      | 1.13                    | 14.04     |
| t4          | 1.13                    | 1.22                    | 7.86      | 0.82                    | 27.37     | 1.28                    | 13.01     | 1.22                    | 7.86      |
| t5          | 0.91                    | 1.04                    | 13.90     | 0.83                    | 8.59      | 0.99                    | 9.29      | 1.04                    | 13.90     |
| t6          | 1.06                    | 1.05                    | 0.89      | 0.46                    | 56.38     | 0.89                    | 16.40     | 1.05                    | 0.89      |
| t7          | 0.93                    | 1.05                    | 12.93     | 0.90                    | 2.71      | 0.89                    | 3.79      | 1.05                    | 12.93     |
| t8          | 0.96                    | 0.82                    | 14.12     | 0.72                    | 24.54     | 0.77                    | 20.04     | 0.82                    | 14.12     |
| t9          | 0.93                    | 0.97                    | 3.89      | 1.53                    | 64.80     | 1.09                    | 17.42     | 0.97                    | 3.89      |
| t10         | 1.48                    | 1.03                    | 30.46     | 1.07                    | 27.90     | 1.03                    | 30.56     | 1.03                    | 30.46     |

<sup>a</sup>FEA results using LS-DYNA.

<sup>b</sup>Predicted values.

PRS: polynomial response surface; RBF: radial basis functions; KR: Kriging; FEA: finite element analysis.

the diameter of the tube is the most influential variable among the other parameters. Figure 9 shows the main effects plot for the springback value with the five input variables (normalized between 0 and 1). None of the variables are found to be insignificant; hence, the surrogate models are constructed in terms of all five variables. If any of the variables were found to be insignificant, those variables could have dropped from the set of variables used in the surrogate models.

### Constructing surrogate models

For constructing the surrogate models, first a group of training points are generated using a design of experiments (DoE) technique and the springback values are computed at these training points. Then, a surrogate model is constructed utilizing the training data. Finally, the prediction of the response at any random point can be achieved using the constructed surrogate model.

### Design of experiments

DoE can be divided into two main categories:<sup>25</sup> (i) classic designs and (ii) space filling designs. Fractional

factorial design, central composite design and Box-Behnken designs<sup>25</sup> are the most generally preferred classic experimental design types. On the other hand, maximum entropy designs,<sup>26</sup> Latin hypercube sampling (LHS) designs,<sup>27</sup> minimax and maximin designs,<sup>28</sup> and orthogonal arrays are the well-known space filling design types. In this study, Taguchi orthogonal arrays DoE is used to keep the computational cost at minimum. L25-Taguchi array (5-factors, 5-levels) is used to create training points provided in Table 3. After generating the training points, the springback values at the training points are computed using LS-DYNA and listed in Column 7 in Table 4.

### Surrogate models

A brief overview about these surrogate models is given in the following sections.

**Polynomial response surface.** PRS models can be customized for any given number of predictor variables  $x_i$  ( $i = 1 \dots L$ ). The most frequently used PRS model is the second-order model defined as follows<sup>29</sup>

$$\hat{y}(x) = b_0 + \sum_{i=1}^L b_i x_i + \sum_{i=1}^L b_{ii} x_i^2 + \sum_{i=1}^{L-1} \sum_{j=i+1}^L b_{ij} x_i x_j \quad (1)$$

where  $\hat{y}$  is the response surface approximations of the actual response function  $f$ ,  $L$  the number of variables in the input vector  $x$ , and  $b_0$ ,  $b_i$ ,  $b_{ii}$ , and  $b_{ij}$  are the unknown coefficients to be determined by the least squares techniques.

**Radial basis functions.** A RBF can be modeled as<sup>30</sup>

$$y(x) = \sum_{i=1}^n \lambda_i \varphi(\|x - x_i\|) \quad (2)$$

where  $\lambda_i$  are unknown interpolation coefficients to be determined,  $n$  the number of data points and  $\varphi$  the RBF of the Euclidean norm from the  $i$ th sampling point, which is the radial distance  $r$  of the design point  $x$  from the sampling point or center  $x_i$

$$r = \|x - x_i\| = \sqrt{(x - x_i)^T (x - x_i)} \quad (3)$$

The unknown coefficients ( $\lambda_i$ ) can be found by minimizing the residual of the deviations formulated as

$$R = \sum_{k=1}^n \left[ f(x_k) - \sum_{i=1}^n \lambda_i \varphi(\|x_k - x_i\|) \right]^2 \quad (4)$$

**Table 10.** Cross-validation errors.

| Case | Data set  | RMSE | MAE  |
|------|---|------|------|
| 1    | 25 training points  | 23.7 | 17.9 |
| 2    | 35 training points (25 original training points combined with 10 test points) | 21.3 | 15.8 |

RMSE: root mean square error; MAE: mean absolute error.

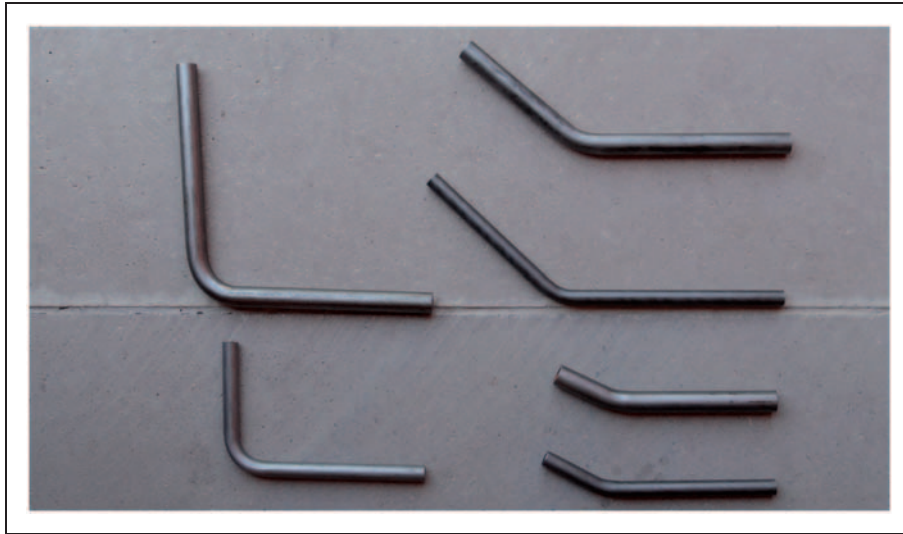


**Figure 10.** CNC rotary-draw tube bender used in the experiments.

CNC: computer numerical control.

**Table 11.** Experimental results for the springback for various geometrical parameters.

| Experimental points | Diameter, $D$ (mm) | Thickness, $t$ (mm) | $R/D$ | Bend angle ( $^{\circ}$ ) | Friction | Springback ( $^{\circ}$ ) |
|---------------------|--------------------|---------------------|-------|---------------------------|----------|---------------------------|
| 1                   | 15                 | 2                   | 2     | 90                        | 0.1      | 1.3                       |
| 2                   | 15                 | 2                   | 2     | 45                        | 0.1      | 1.1                       |
| 3                   | 15                 | 2                   | 2     | 30                        | 0.1      | 1.4                       |
| 4                   | 20                 | 4                   | 2     | 90                        | 0.1      | 2.2                       |
| 5                   | 20                 | 4                   | 2     | 45                        | 0.1      | 1.3                       |
| 6                   | 20                 | 4                   | 2     | 30                        | 0.1      | 1.0                       |

**Figure 11.** Sample tubes having different geometrical properties bended using CNC rotary-draw tube bender. CNC: computer numerical control.

In this study, multi-quadratic formulation  $\varphi(r) = \sqrt{r^2 + c^2}$  with  $c = 1$  is used, as suggested in the study of Wang et al.<sup>31</sup>

**Kriging.** A KR model basically assumes a synthesis of a trend model and stochastic component of the form

$$\hat{y} = \sum_{i=1}^k \beta_i f_i(x) + Z(x) \quad (5)$$

where the trend model globally approximate the response and  $Z(x)$ , the stochastic component creates deviations with mean zero and covariance

$$\text{COV}[Z(x_i), Z(x_j)] = \sigma^2 \mathbf{R}[R(x_i, x_j)] \quad (6)$$

where  $\sigma^2$  is the process variance and  $\mathbf{R}$  the  $N \times N$  correlation matrix;  $N$  is the number of sampling points. The term  $R(x_i, x_j)$  is the correlation function between

two sampling points  $x_i$  and  $x_j$ . In this study, the trend model is chosen as constant and the correlation model is chosen as Gaussian as suggested by Simpson et al.<sup>32</sup> The MATLAB<sup>®</sup> KR toolbox developed by Lophaven et al.<sup>33</sup> is used in this study.

### Accuracy of surrogate models

The accuracies of the constructed surrogate models are estimated at various test points (Table 6) generated using LHS technique. Note that these test points are not used while fitting the surrogate models. Springback values at the test points are compared to the predicted springback values of the response using the surrogate models (Table 7). After computing the error values for each test point (Table 8), root mean square error (RMSE) and mean absolute error (MAE) metrics are calculated from these results (Table 9). As seen from

Table 9, error metrics for the linear PRS are the smallest.

The constructed linear PRS model (using 25 training points) is given in equation (7)

$$\hat{s}_b = 1.1334 - 0.0122D - 0.0009t + 0.0976(R/D) + 0.0045\theta - 0.0320f_s \quad (7)$$

Recall that we first generated 25 training points, constructed the surrogate models, generated 10 test points and evaluated the accuracy of surrogate models using the test points. The accuracies of constructed surrogate models can also be assessed using leave-one-out cross-validation error metrics. The cross-validation error is calculated as follows. A surrogate model is constructed  $N$  times with  $N-1$  training points, each time one of the training points is reserved as the validation data for testing the accuracy of the model. Then, RMSE and MAE metrics (%) are calculated as given in equations (8) and (9), respectively

$$\text{RMSE} = \sqrt{\frac{1}{N} \sum_{i=1}^N \left( \frac{y_i - \hat{y}_{(i)}}{y_i} \times 100 \right)^2} \quad (8)$$

$$\text{MAE} = \frac{1}{N} \sum_{i=1}^N \left| \frac{y_i - \hat{y}_{(i)}}{y_i} \times 100 \right| \quad (9)$$

where  $y_i$  is the exact value of the response at the retained training point  $x_i$  and  $y_{(i)}$  the predicted value of the response using surrogate model.

Table 10 presents accuracy evaluation of surrogate models for two different cases. In the first case, the leave-one-out cross-validation error values are computed using 25 training points for the linear PRS model. It is seen by comparing Tables 9 and 10 that the cross-validation errors are larger than the errors evaluated at test points. The second case indicates the cross-validation error when 10 test points are merged with 25 training points to get a data set of 35 points. It is seen that this operation reduced the cross-validation errors. Therefore, a new linear PRS model is constructed using the data set of 35 points. The constructed linear PRS model (using 35 data points) is given in equation (10). It can be argued that if 10 more test points were generated and the accuracy of this new linear model PRS were evaluated at those test points, the RMSE and MAE of the new linear model would be smaller than those provided in Table 9.

$$\hat{s}_b = 1.0096 - 0.0109D - 0.0023t + 0.0984(R/D) + 0.0051\theta + 0.1739f_s \quad (10)$$



**Figure 12.** Springback measurement from a sample. Material: A573-81 65, bend angle ( $\theta$ ):  $90^\circ$ , bend radius ( $R$ ): 30 mm, tube diameter ( $D$ ): 15 mm, and tube thickness ( $t$ ): 2 mm.

## Comparison of experimental and numerical results

The CNC rotary-draw tube bender used in the experiments is shown in Figure 10. The experiments are conducted using the tubes having the same mechanical properties given in Table 2. The tubes used in the experiments have different thicknesses and bended for various bend angles (Table 11). The bended tube shapes after the experiments can be seen in Figure 11. The springback angles are measured in CATIA using the digital photographs of the bended tubes, as shown in Figure 12. Six different geometrical parameters are used in the experiments. The geometrical properties of the samples used in the experiments, the bending angles, and the springback results obtained for different experiments are presented in Table 11.

The comparison between the experimental results and the PRS models using 25 training points (equation 7) and 35 training points (equation 10) is given in Table 12, which also shows the percentage error between the numerical and experimental results. It is observed that as the number of training points increases, the error in springback prediction decreases. It is seen that the mean absolute error is reduced from 18.7% to 16.9%. In addition, comparing the errors reported in Tables 10 and 12, it is seen that the cross-validation error predictions are in line with the errors observed in experiments. The reason for these errors might be due to the clearance between the tube and the dies, misalignment of the tube when it is mounted by the operator to the bender, the machine setting (the radial and axial pressures applied by the pressure die to the tube), and the placement of the mandrel nose relative to the line of tangency.

**Table 12.** Comparison between experimental and numerical springback results.

| Experimental points | Springback (°) experiment | Springback (°) equation (7) | Error (%) equation (7) | Springback (°) equation (10) | Error (%) equation (10) |
|---------------------|---------------------------|-----------------------------|------------------------|------------------------------|-------------------------|
| 1                   | 1.30                      | 1.63                        | 25.12                  | 1.51                         | 16.51                   |
| 2                   | 1.10                      | 1.38                        | 25.78                  | 1.29                         | 16.84                   |
| 3                   | 1.40                      | 1.30                        | 6.96                   | 1.21                         | 13.67                   |
| 4                   | 2.20                      | 1.56                        | 28.92                  | 1.46                         | 33.84                   |
| 5                   | 1.30                      | 1.32                        | 1.60                   | 1.23                         | 5.69                    |
| 6                   | 1.00                      | 1.24                        | 23.98                  | 1.15                         | 14.96                   |
|                     |                           | MAE                         | 18.73                  |                              | 16.92                   |

MAE: mean absolute error.

## Conclusions

In this study, we investigated springback phenomena in rotary-tube bending process involving interactions between the geometrical and mechanical variables. For that purpose, the main tools of a typical rotary-draw tube bending machine were modeled and simulations were performed explicitly using non-linear FE code LS-DYNA. ANOVA techniques were utilized to determine the most influential parameters. Surrogate models are constructed to obtain fast springback predictions for a given combination of the parameters. From the results of this study, the following conclusions can be drawn.

1. Springback simulations were performed for different bend angles and it was found that the magnitude of the springback increases almost linearly with increasing bend angle.
2. Tube diameter was found to be the most effective parameter and the springback linearly decreases with increasing diameter.
3. Increasing the tube thickness reduces the springback.
4. Increasing the bend radius increases the amount of area that elastically deformed, and thus causes an increase in the springback.
5. As the coefficient of friction increases, the springback increases rather non-linearly.
6. Three different surrogate modeling techniques were utilized: PRSs, RBFs, and KR. It was found that the linear PRSs provided the most accurate springback predictions.
7. Experiments were conducted to validate the accuracy of surrogate models. It was seen that the cross-validation error predictions were in line with the errors observed in experiments.

Future research may focus on the use of meshfree methods to study the springback behavior on rotary-tube bending process.

## Funding

This work was supported by the Scientific and Research Council of Turkey (TUBITAK) [grant number MAG-109M078].

## Acknowledgments

The authors wish to acknowledge M. Fatih Aycan of Republic of Turkey Ministry of Science, Industry and Technology, and Ulrich Stelzmann of CADFEM, Recep M. Görgülüarslan and Engin M. Kaplan of TOBB University of Economics and Technology for their contributions to this study. The authors also acknowledge the support provided by DOĞANER MAKİNA and ÖZ AKSEN OTOMOTİV for sharing the experimental facilities.

## References

1. Miller GG. *Tube forming processes - a comprehensive guide*. Dearborn, MI: Society of Manufacturing Engineers, 2003.
2. Mentella A, Strano M and Gemignani R. A new method for feasibility study and determination of the loading curves in the rotary draw-bending process. *Int J Mater Form* 2008; 1: 165–168.
3. Pan K and Stelson KA. On the plastic deformation of a tube during bending. *Trans ASME J Eng Ind* 1995; 117(4): 494–500.
4. Shr SG. *Bending of tubes for hydroforming: A state of the art review and analysis*. Master Thesis, Graduate School of the Ohio State University, Ohio, 1998.
5. Khodayari G. How the material influences the bending for hydroforming: Effects on ovality springback and wall thickness in tubes. *Tube Pipe Journal*, <http://www.thefabricator.com/article/hydroforming/how-material-influences-bending-for-hydroforming> (2002, accessed 27 February 2012).
6. Wang JW and Agarwal R. Tube bending under axial force and internal pressure. *Trans ASME J Manuf Sci Eng* 2006; 128: 598–605.
7. Dohmann F and Hartl C. Hydroforming-applications of coherent FE-simulations to the development of products and processes. *J Mater Process Technol* 2004; 150: 18–24.

8. Grantab R. *Interaction between forming and crashworthiness of advanced high strength steel*. Master Thesis, Department of Mechanical Engineering, University of Waterloo, Waterloo, ON, 2006.
9. Sorine M. *Formability of advanced of high strength steel tubes in tube bending and hydroforming*. Master Thesis, Department of Mechanical and Mechatronics Engineering, University of Waterloo, Waterloo, ON, 2007.
10. Li H, Yang H, Zhan M, et al. Role of mandrel in NC precision bending process of thin-walled tube. *Int J Mach Tools Manuf* 2007; 47(7–8): 1164–1175.
11. Li H, Yang H, Yan J, et al. Numerical study on deformation behaviors of thin-walled tube NC bending with large diameter and small bending radius. *Comput Mater Sci* 2009; 45: 921–934.
12. Yang H, Yan J, Zhan M, et al. 3D numerical study on wrinkling characteristics in NC bending of aluminum alloy thin-walled tubes with large diameters under multi-die constraints. *Comput Mater Sci* 2009; 45: 1052–1067.
13. Zhao GY, Liu YL, Yang H, et al. Three-dimensional finite-elements modeling and simulation of rotary-draw bending process for thin-walled rectangular tube. *Mater Sci Eng A* 2009; 499: 257–261.
14. Song N, Qian D, Cao J, et al. Effective models for prediction of springback in flanging. *ASME J Eng Mater Technol* 2001; 123(4): 456–461.
15. Liu H, Xing Z, Sun Z, et al. Adaptive multiple scale meshless simulation on springback analysis in sheet metal forming. *Eng Anal Boundary Elem* 2001; 35(3): 436–451.
16. Gu RJ, Yang H, Zhan M, et al. Springback of thin-walled tube NC precision bending and its numerical simulation. *Trans Nonferrous Met. Soc. China* 2006; 16: 631–638.
17. Gu RJ, Yang H, Zhan M, et al. Research on the spring-back of thin-walled tube NC bending based on the numerical simulation of the whole process. *Comput Mater Sci* 2008; 42(4): 537–549.
18. Da-xin E, Hua-Hui H, Xiao-Yi L, et al. Spring-back deformation in tube bending. *Int J Miner Metall Mater* 2009; 16(2): 177–183.
19. Lou H and Stelson KA. Three-dimensional tube geometry control for rotary draw tube bending, part 1: bend angle and overall tube geometry control. *Trans ASME J Manuf Sci Eng* 2001; 123: 258–265.
20. Lou H and Stelson KA. Three-dimensional tube geometry control for rotary draw tube bending, part 2: statistical tube tolerance analysis and adaptive bend correction. *Trans ASME J Manuf Sci Eng* 2001; 123: 266–271.
21. ANSA BETA-CAE Systems. *User's guide*, Thessaloniki, Greece: ANSA BETA-CAE Systems, 2008.
22. Livermore Software Corporation. *Ls-dyna keyword user's manual*. Ver. 971. Livermore, CA: Livermore Software Corporation, 2010.
23. Maker BN and Zhu X. *Input parameters for springback simulation using LS-DYNA*. Livermore, CA: Livermore Software Technology Corporation, 2001.
24. The MathWorks Inc. *MATLAB user's guide and reference guide*. Natick, MA: The MathWorks Inc., 2007.
25. Wang GG and Shan S. Review of metamodeling techniques in support of engineering design optimization. *J Mech Des* 2007; 129(4): 370–380.
26. Currin C, Mitchell TJ, Morris MD, et al. Bayesian prediction of deterministic functions, with applications to the design and analysis of computer experiments. *J Am Stat Assoc* 1991; 8: 953–963.
27. Park JS and Stat J. Optimal latin-hypercube designs for computer experiments. *J Stat Plan Inference* 1994; 39: 95–111.
28. Johnson ME, Moore LM and Ylvisaker D. Minimax and maximin distance designs. *J. Stat Plan Inference* 1990; 26(2): 131–148.
29. Myers RH and Montgomery DC. *Response surface methodology: process and product optimization using designed experiments*. New York, NY: Wiley, 2002.
30. Buhmann MD. *Radial basis functions: theory and implementations*. New York, NY: Cambridge University Press, 2003.
31. Wang L, Beeson D, Wiggs G, et al. *Comparison of meta-modeling methods using practical industry requirements*. paper no. AIAA-2006-1811, 2006. Reston, VA: AIAA.
32. Simpson TW, Mauery TM, Korte JJ, et al. Comparison of response surface and Kriging models for multidisciplinary design optimization. In: *Proceedings of the 7th AIAA/USAF/NASA/ISSMO symposium on multidisciplinary analysis and Optimization*, St. Louis, MO, 2–4 September 1998, paper no. AIAA-98-4755, Collection of Technical Papers, Pt. 1 (A98-39701 10-31). Reston, VA: AIAA.
33. Lophaven SN, Nielsen HB and Søndergaard J. *DACE-a MATLAB kriging toolbox, informatics and mathematical modeling*. Lyngby: Technical University of Denmark, 2002.